JACS
JOURNAL OF THE AMERICAN CHEMICAL SOCIETY
pubs.acs.org/JACS
Article

A Robust Single-Molecule Diode with High Rectification Ratio and Integrability

Yilin Guo,[⊥] Chen Yang,[⊥] Shuyao Zhou,[⊥] Kendall N. Houk,* and Xuefeng Guo*

Cite This: J. Am. Chem. Soc. 2025, 147, 16972−16981

ABSTRACT: Advancements in molecular electronics focus on single molecules as key components to create stable and functional devices that meet the requirements of device miniaturization and molecular function exploration. However, as the pioneering concept of a molecular diode, all single-molecule rectifiers reported previously are limited by their modest rectification ratios, owing to electron transmission in the off-state, highlighting the imperative for performance enhancements. Here, we demonstrate a unique method capable of realizing a stable and reproducible high-performance single-molecule rectifier through the strategic application of an electric-field-catalyzed Fries rearrangement. This flexible reaction enables the exquisite control of reversible conductance switching between a structure with constructive quantum interference and a structure with destructive quantum interference, therefore leading to an exceptional rectification ratio of up to 5000 at a bias of 1.0 V, which ranks the highest among the rectifiers constructed by only one individual molecule. The stable operation of nearly 100 devices at high temperatures demonstrates reproducibility. Moreover, on-chip integration of different single-molecule rectifiers succeeds in achieving half-wave and bridge rectifications, thus facilitating efficient alternating current-to-direct current conversions. This convenient strategy of electric-field-catalyzed quantum interference switching potentially revolutionizes device efficiency and miniaturization in nanotechnology, laying an actual step toward future practical integrated molecular-scale electronic nanocircuits.

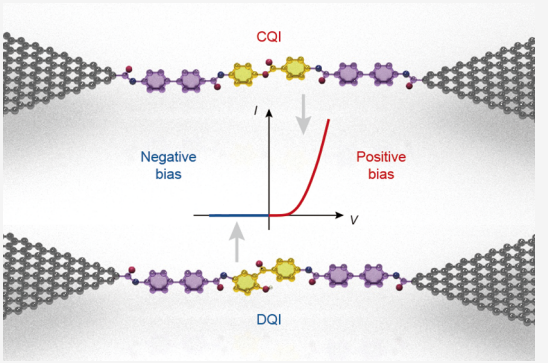

INTRODUCTION

In the pursuit of miniaturizing electronic components, the ultimate goal is to harness single molecules as components of stable and functional electronic devices. The expansion from conventional electronics to molecular building blocks not only signifies further miniaturization of electronic devices but also paves the way for the exploration of unique molecular functionalities.[1−5] Due to the ultimate physical size and unique properties, single-molecule building blocks hold immense potentials for the evolution of future electronic devices.[6] One of the most fundamental electronic components is the diode. The construction of a reliable molecular diode would be a crucial test for evaluating the usefulness of molecular electronics in conventional circuit architectures. In 1974, Aviram and Ratner proposed a theoretical landmark for a molecular rectifier, featuring donor and acceptor moieties separated by a σ-bridge.[7] This pioneering model leveraged the asymmetric charge flow resulting from the intramolecularly uneven charge distribution. Since the inception of this concept, scientists have made tremendous efforts to fabricate molecular rectifiers.[8−12] The central aspect of molecular rectification lies in the asymmetry along the direction of charge transport in the electrode−molecule−electrode junction (Figure 1a). Various strategies (Figure 1b) have been employed to break the symmetry, including asymmetric molecular cores,[13−19] anchoring groups,[20−22] electrodes,[23−25] asymmetric environments,[26] and spatial variations induced by molecular intercalation.[27] At present, for multiple molecular systems, a high rectification ratio (RR) of up to 10^5 has been achieved,[28] which is comparable to those of CMOS devices. However, for an individual molecule, most reported RRs are relatively modest due to the reverse tunneling leakage current.[8] Therefore, the development of robust single-molecule rectifiers with high RRs remains a formidable challenge.

The RR is not the only performance metric for rectifiers; efficient alternating current (AC)-to-direct current (DC) conversion is also crucial. Half-wave and bridge rectifiers are both critical in AC-to-DC conversion, a fundamental process for powering electronic devices, battery charging, and large-scale power systems. Scaling down to the molecular scale presents revolutionary opportunities for developing modern integrated circuits with compact and efficient power conversion. Therein,

Received: January 16, 2025
Revised: April 8, 2025
Accepted: April 8, 2025
Published: April 17, 2025

https://doi.org/10.1021/jacs.5c00566
J. Am. Chem. Soc. 2025, 147, 16972−16981

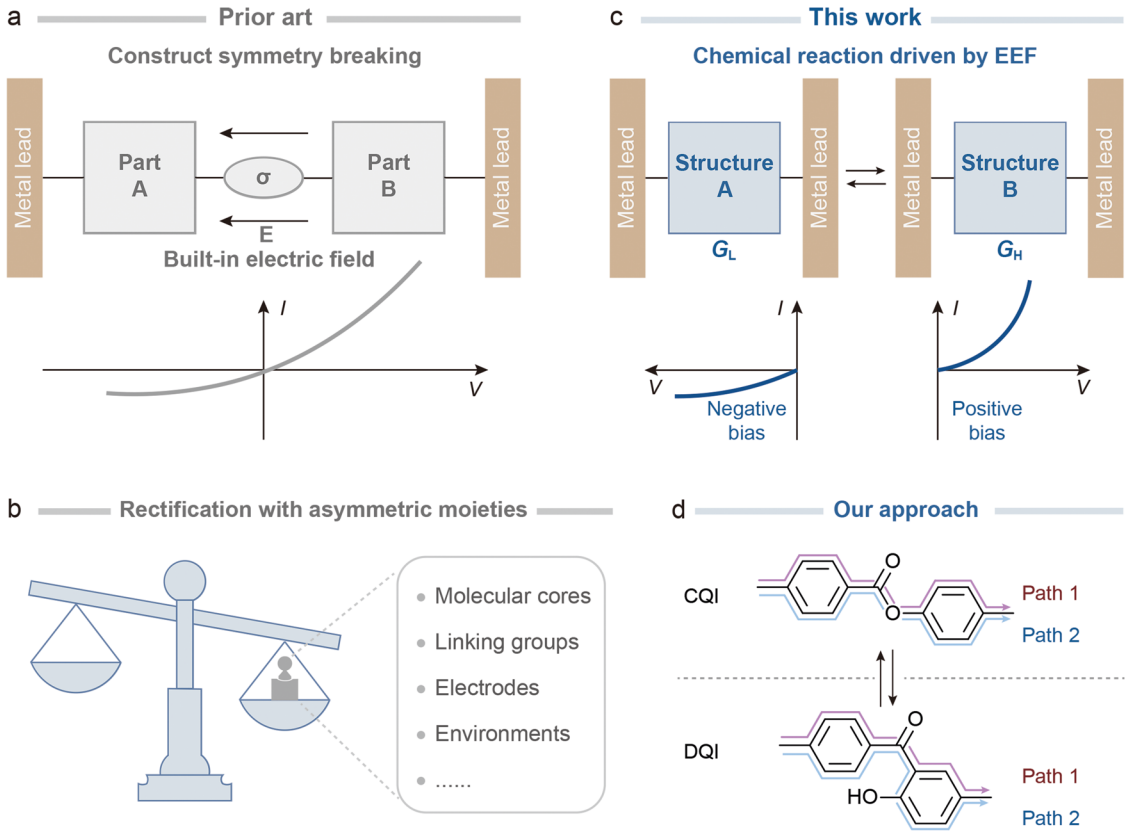

Figure 1. Strategies for the fabrication of single-molecule rectifiers. (a) Schematic of the approaches employed in previous research for constructing single-molecule rectifiers, which hinges on the introduction of symmetry-breaking elements. (b) Schematic of the asymmetric elements to achieve symmetry breaking in single-molecule junctions, including molecular cores, linking groups, electrodes, and environmental factors. (c) Schematic of the approach presented in this study, showcasing a method to achieve stable and reproducible rectification by strategically applying electric-field-catalyzed reactions to stabilize two structures that exhibit substantial conductance differences under opposing electric field orientations. (d) Schematic of the two structures involved in the Fries rearrangement. Top panel: substrate exhibiting constructive quantum interference (CQI); bottom panel: product exhibiting destructive quantum interference (DQI).

constructing half-wave and bridge rectifiers at the single-molecule level is a cutting-edge pursuit, reflecting a significant stride in the miniaturization of electronic components. Tremendous efforts have been made in the development of state-of-the-art half-wave and full-wave rectifying circuits based on large-area junctions.[29−31] However, achieving similar functionality with single-molecule rectifiers remains challenging due to the limitations in preparation techniques and device stability.

To address these challenges, a strategy of introducing constructive quantum interference (CQI) under the forward bias and destructive quantum interference (DQI) under the reverse bias was proposed to construct molecular rectifiers. Quantum interference effects (QIEs) rely strongly on the connectivity patterns. Regarding the highly conjugated molecular wire, the theory predicts[32] that benzene systems with *meta*-connectivity have lower conductance than those with *para*-/*ortho*-connectivity because of DQI, which has been experimentally confirmed.[33] Switching between the *meta*-connectivity and *para*-/*ortho*-connectivity through chemical reactions offers a feasible approach. In other words, constructing single-molecule rectifiers in this way necessitates a robust structural rearrangement of the molecular bridge. The two possible reactions are Claisen and Fries rearrangements that occur on the benzene ring, which pose a significant challenge in constructing most single-molecule junctions. Using graphene as electrodes and covalently bonded electrode−molecule interface offers high stability, including the endurance of high voltage and complicated solvent environment, to implement chemical reactions on single-molecule junctions, which have been validated systematically[34−36] and might address this challenge.

In this study, by taking advantage of the rearrangement reversibility, we utilize the directional selectivity of an electric field in the Fries rearrangement to stabilize *para*-connected aromatic systems (substrate) under the forward bias and *meta*-connected aromatic systems (product) under the reverse bias, leading to the reproducible and stable rectification performance (Figure 1c,d). Another benefit of this strategy is that the rectification ratio can be adjusted by modulating the substrate and product separately. An RR exceeding 700 can be achieved with a bias of 1 V, with the value further increasing to more than 3000 under a 2 V bias. Moreover, with the assistance of Lewis acid to enhance DQI, the rectification performance of single-molecule rectifiers was significantly improved, yielding an RR value exceeding 5000 at a bias of 1 V. In addition, we showcase the half-wave rectification performance of the system, demonstrating a robust AC-to-DC conversion. Taking it a step further, we successfully integrated four single-molecule rectifiers and built a bridge rectifier on a single chip, exhibiting the capability of full-wave rectification. This development highlights the potential of these devices for enhancing efficiency and miniaturizing electronic components. It also lays a solid

https://doi.org/10.1021/jacs.5c00566
J. Am. Chem. Soc. 2025, 147, 16972−16981

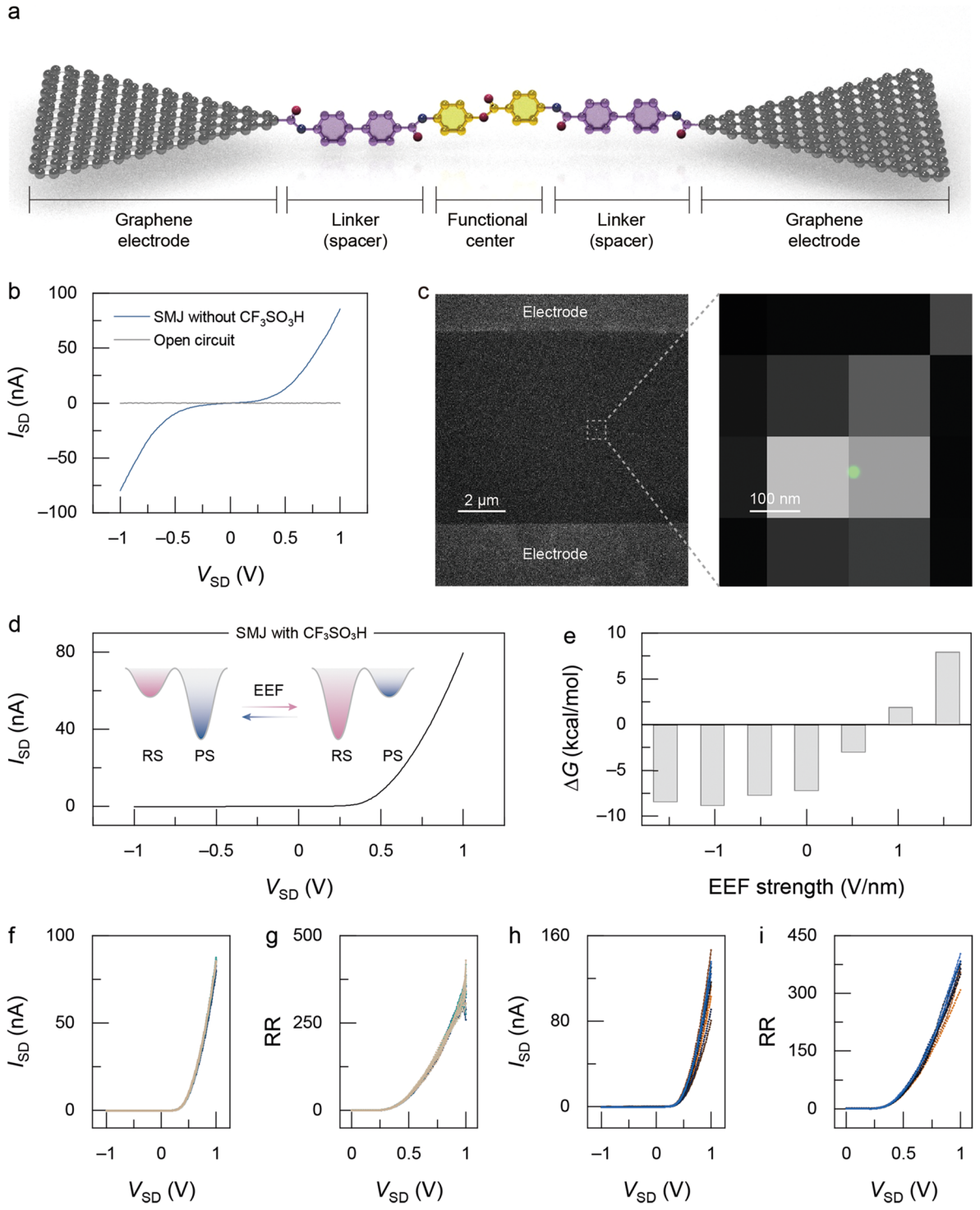

Figure 2. Construction and characterization of single-molecule rectifiers. (a) Schematic of a single-molecule junction with the phenyl benzoate center. (b) *I*−*V* curves of open circuits with graphene point contacts (gray) and single-molecule junctions without solvent after the molecular connection (blue). The signals indicate the successful formation of single-molecule junctions. (c) Optical characterization of the single-molecule junction. The right panel shows only one bright spot in the superhigh-resolution image obtained by the stochastic optical reconstruction microscopy technology, again proving the success in forming single-molecule junctions. Laser: 405 nm, 5 mW. Five thousand photos were taken through a ×100 oil lens with an exposure time of 50 ms. (d) *I*−*V* curves of a single-molecule junction with the addition of CF_3SO_3H (1×10^{-5} mol/L) in *N*,*N*-dimethylformamide solution. Inset: energy level diagrams of the reactant state (RS) and product state (PS) under the external electric field (EEF). (e) Computational results of the energy difference between RS and PS under different EEF strengths. $\Delta G = G(\mathrm{PS}) - G(\mathrm{RS})$. (f) *I*−*V* curves (28 traces) in the same device without data selection at 363 K. (g) Corresponding rectification ratio (RR) vs bias voltage of *I*−*V* curves shown in panel (f). (h) *I*−*V* curves of 10 devices at 363 K. (i) Corresponding RR−*V* curves of *I*−*V* curves shown in panel (h).

foundation for exploration and innovation in future integrated electronic applications.

https://doi.org/10.1021/jacs.5c00566
J. Am. Chem. Soc. 2025, 147, 16972−16981

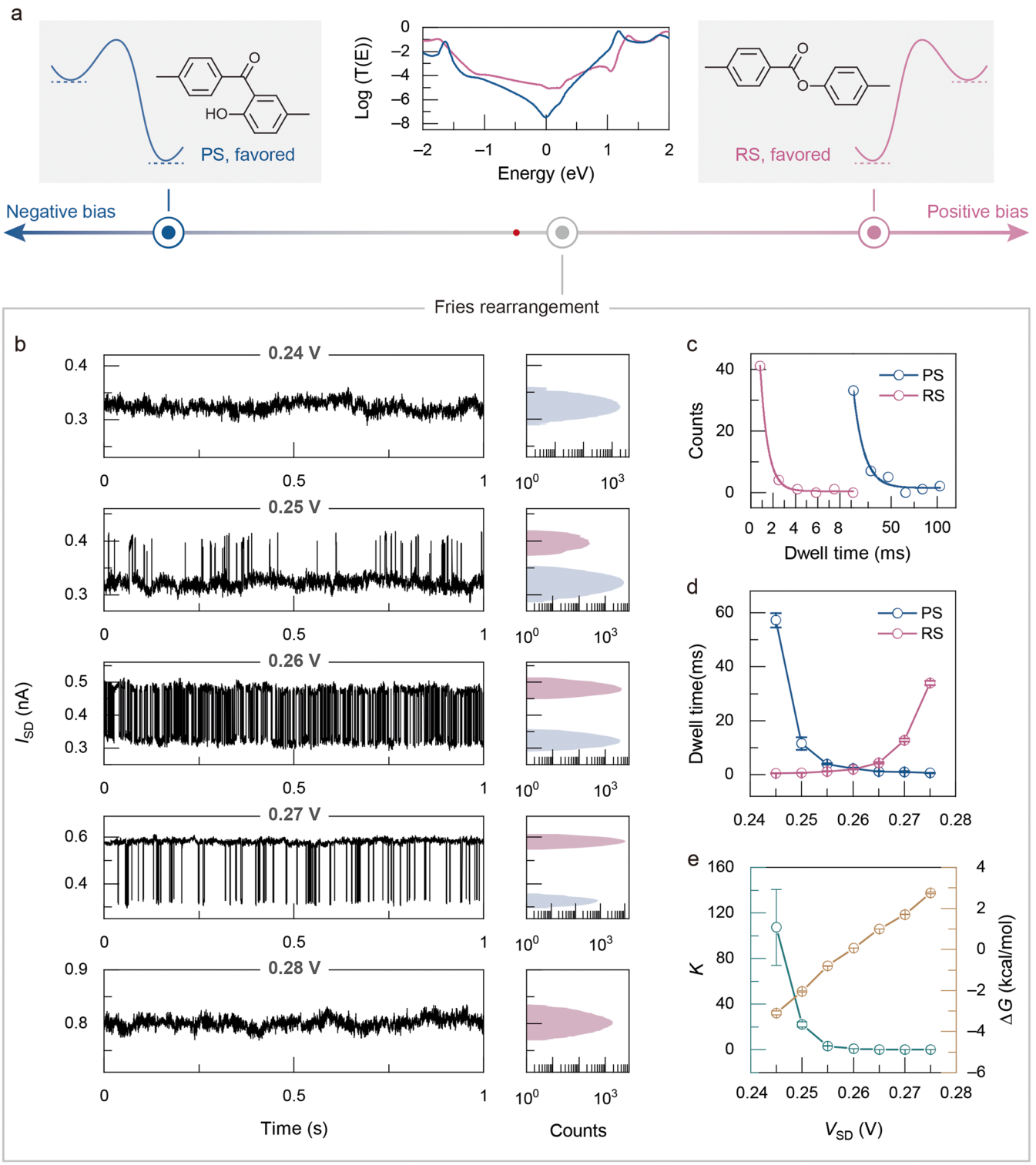

Figure 3. Rectification mechanism of the single-molecule rectifier. (a) Transmission spectra of RS and PS, and schematics of the energy profiles under the opposing electric field directions. (b) $I-t$ curves and corresponding histograms in bias-voltage-dependent measurements. (c) Plots of time intervals at 0.25 V. The dwell times of the low conductance state (PS) and the high conductance state (RS) in panel (d) were obtained from the single-exponential fittings. (d) Dwell times of RS and PS versus bias voltage. (e) Equilibrium constant (K) of the reaction and corresponding ΔG versus bias voltage.

RESULTS AND DISCUSSION

Device Fabrication and Characterization. The graphene point electrodes with carboxyl terminals on a SiO_2/Si substrate were obtained by oxygen plasma etching and supplemental electrical burning. The terminals were premodified with 4′-amino-biphenyl-4-carboxylic acid to further shorten the nanogap length between graphene electrodes, which is more compatible with the functional center having a short molecular length. Then, the amine-terminated functional center (4-aminobenzoic acid 4-aminophenyl ester) was integrated into

https://doi.org/10.1021/jacs.5c00566
J. Am. Chem. Soc. 2025, 147, 16972−16981

the suitable gap by the formation of amide bonds to form a graphene−molecule−graphene single-molecule junction (Figure 2a and Scheme S1). The detailed fabrication of single-molecule devices is provided in the Supporting Information (Section S2). The recovery of the current−voltage ($I-V$) response exhibits the successful incorporation of the functional center (Figure 2b). Under optimized conditions, the connection yield reached ∼18%, with ∼30 of the 169 devices on the same silicon chip showing the recovery of conductance (Figures S1 and S2). The statistical analysis was performed (Section S4, Figure S3), showing that the probability of electrical signals originating from only one molecule connection between electrodes is ∼99%, which was further supported by the superhigh-resolution imaging (Figure 2c).

Rectification Performance. To construct a single-molecule rectifier via QIEs, Fries rearrangement was chosen as the approach to facilitate the transformation between the aromatic systems with different connectivities. Green's function,[37,38] serving as a measure for the interconnected pathways established by the molecular bonding patterns,[39] can be written as follows (left panel)

$$G_{ij}(E_F) = \sum_k \frac{C_{ik}C_{jk}^*}{E_F - \varepsilon_k \pm i\eta} \approx \frac{C_{i\mathrm{HOMO}}C_{j\mathrm{HOMO}}^*}{E_F - \varepsilon_{\mathrm{HOMO}} \pm i\eta} + \frac{C_{i\mathrm{LUMO}}C_{j\mathrm{LUMO}}^*}{E_F - \varepsilon_{\mathrm{LUMO}} \pm i\eta} \quad (1)$$

where E_F represents the Fermi level, C_{rk} denotes the kth molecular orbital coefficient at site r, asterisk signifies a complex conjugate, ε_k denotes the kth molecular orbital energy, and η is an infinitesimal positive number. By exclusively considering the highest occupied molecular orbital (HOMO) and lowest unoccupied molecular orbital (LUMO) and assuming that E_F lies between HOMO and LUMO, Green's function can be further approximated as shown in the right panel of the equation. Consequently, the increase (decrease) in $|G_{ij}(E_F)|$, corresponding to CQI (DQI), arises from the same (opposite) signs of the two terms. For the benzene system, it can be predicted that CQI occurs for *para*-connectivity (owing to the same signs) and DQI for *meta*-connectivity (owing to the opposite signs), which has been confirmed by both theoretical[32] and experimental validations.[33] As shown in Figure 1d, the reactant state (RS) of the Fries rearrangement, i.e., phenyl benzoate bearing a *para*-substituted phenyl ring along the electron transmission paths, exhibits CQI. Conversely, for the product state (PS), which bears a *meta*-substituted phenyl ring, the unequal path lengths around the phenyl ring result in DQI. This was further supported by the transmission spectra (Figures S6 and 3a), showing a conspicuous sharp dip around the Fermi level. The detailed computational analysis of QIEs on RS and PS is provided in the Supporting Information (Section S5, Figures S4−S6, and Tables S1−S4).

As the catalyst of the Fries rearrangement, CF_3SO_3H (1×10^{-5} mol/L) in *N*,*N*-dimethylformamide solution was added to the laboratory-built reaction cell covering the molecular bridge. In comparison with the measured current without the catalyst, which shows a symmetrical response to voltage (Figure 2b), the $I-V$ curve in the presence of CF_3SO_3H exhibits obviously asymmetrical behavior under the forward and reverse biases at 363 K (Figure 2d). Due to the random orientations of the molecules connecting the electrodes, $I-V$ curves with the opposite rectification direction were also observed (Figure S7). In the range from −1 to +0.3 V, the conductance of single-molecule junctions (SMJs) remains in a low state with a scale of $\sim 10^{-10}$ S. However, under biases exceeding ∼0.3 V, the conductance of SMJs increased to a scale of $\sim 10^{-8}$ S, representing a two-order-of-magnitude enhancement. Supported by the computational simulations (Figures 2e and S8−S14), the observed rectification behavior was attributed to the influence of the external electric field (EEF) on the reactivity of Fries rearrangement (*vide infra*), which suppresses the reaction at the forward bias and facilitates it at the reverse bias. This can be attributed to the orientation of the reaction axis versus the electric field (*vide infra*). Therefore, the functional center of SMJs remained in the RS under the high positive bias and in the PS under the high negative bias. Figure 2f shows 28 traces of $I-V$ scans in the same device without data selection (363 K), demonstrating the high uniformity and stability of the single-molecule rectifier. The corresponding rectification ratios (RRs) under the varying biases are provided in Figure 2g, yielding an average RR of ∼351 at ±1 V. Furthermore, rectification behaviors were also observed in additional devices (Figure 2h,i), underscoring the reproducibility of single-molecule rectification.

Rectification Mechanism. The impact of EEFs on the energy profile of the Fries rearrangement was simulated to elucidate the rectification phenomenon, as illustrated in Figures S8−S14. It was observed that the strength and direction of the electric field, which were parallel or antiparallel to the direction of the molecular bridge, had a regular and obvious influence on the energy profile of the reaction (Figure 2e). Specifically, in the absence of EEF, the relative Gibbs free energies of RS and PS were approximately 0.0 kcal/mol and −7.2 kcal/mol, respectively. However, with the application of a strong forward EEF, the energy level of PS significantly increased to approximately +7.9 kcal/mol, indicating a reversal in the occupancy of RS and PS. Conversely, under the reverse EEF, the Gibbs free-energy level of PS decreased to −8.4 kcal/mol, demonstrating the dominance of PS. This regulation of Fries rearrangement through the EEF facilitated the stabilization of RS under the high forward bias and PS under the reverse bias, ultimately leading to the observed rectification behaviors (Figure 3a). Note that the turning point of the current change (RR > 1) was not the traditional 0 V but rather approximately 0.3 V.

To provide a detailed mechanical picture of the kinetic and thermodynamic information, the $I-t$ characterization was conducted within the bias range of around 0.3 V (353 K), as shown in Figures 3b and S15 (electrical signals of two other different devices are provided in Figures S16 and S17). Bias-voltage-dependent measurements revealed a binary switching between two conductance states within the range from 0.24 to 0.28 V, indicating the transition zone that delineates RS and PS. In combination with the transmission spectra (Figures S6 and 3a), the high conductance state was attributed to the RS, while the low conductance state was assigned to the PS. The control experiment conducted with another molecular bridge containing the biphenyl functional center (Scheme S2) exhibited no obvious fluctuations (Figure S18), indicating that the binary switching originates from the reconstruction of phenyl benzoate. In addition, inelastic electron tunneling spectroscopy characterizations of the two conductance states are provided in Figures S19 and S20, further supporting the occurrence of the Fries rearrangement and the assignments of the conductance states. Furthermore, the corresponding histograms (Figure 3b, right

https://doi.org/10.1021/jacs.5c00566
J. Am. Chem. Soc. 2025, 147, 16972−16981

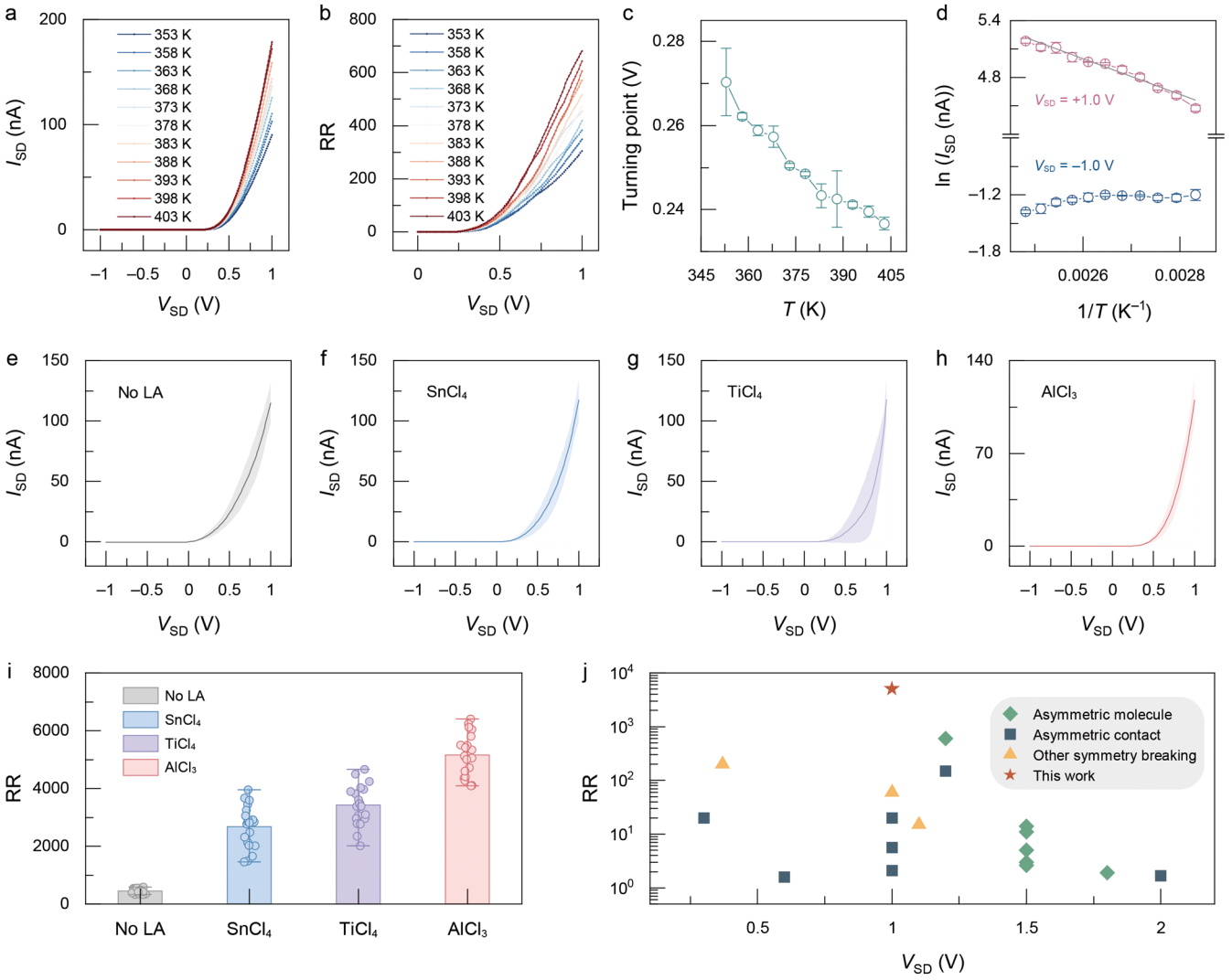

Figure 4. Regulation of rectification performance. (a) $I-V$ curves in temperature-dependent measurements. (b) Corresponding RR versus bias voltage in temperature-dependent measurements. (c) Bias at the turning point versus temperature. (d) Plots of ln (I_{SD}) versus $1/T$ at +1.0 V (red) and −1.0 V (blue). The gray curve represents the linear fitting to ln (I_{SD}) versus $1/T$ at +1.0 V. (e) Statistically averaged $I-V$ curves of 20 devices without the addition of a Lewis acid (LA). Gray shadow: error band. (f) Statistically averaged $I-V$ curves of 20 devices with the addition of $SnCl_4$. Blue shadow: error band. (g) Statistically averaged $I-V$ curves of 20 devices with the addition of $TiCl_4$. Purple shadow: error band. (h) Statistically averaged $I-V$ curves of 20 devices with the addition of $AlCl_3$. Red shadow: error band. (i) Corresponding RR values of multiple devices in the Lewis-acidity-dependent measurements. (j) Comparison of the rectification performance of our rectifier with previously reported results.[13−27,42] The rectifiers in these references are all one-individual-molecule setups; that is, there is no intermolecular cooperation.

panel) demonstrated that RS and PS exhibited opposite preferences in response to the strength of the electric field, which was consistent with the $I-V$ scan and the computational simulation. This opposing trend was also evident in the dwell times (τ) of the two states (Figure 3d), which were obtained through the single-exponential fitting of the time intervals (Figures 3c and S21). The short lifetimes (submillisecond, determined by the measurement time resolution) of RS (PS) at 0.24 V (0.28 V) imply a fast response to the bias, especially the alternating voltage, enabling an AC-to-DC conversion. The thermodynamics also supports this. The equilibrium constant (K) of the reaction, derived from the ratios of the peak areas in the histograms, decreased with increasing biases, indicating the complete suppression of the forward reaction (Figure 3e, green curve). The corresponding calculated $\Delta G = (G(\mathrm{PS}) - G(\mathrm{RS}))$ versus bias voltage was obtained by $\Delta G = -RT \ln K$ (Figure 3e, yellow curve), which is in line with the computational simulation (Figure 2e). In summary, the fast dynamics and strong dependence of the equilibrium on the EEF determine the high-frequency and robust performance of single-molecule rectifiers.

Regulation of the Rectification Ratio. Different temperature-dependent electron transport modes of substrates and products make the rectification ratio temperature-tunable (Figure 4a). As the temperature increased from 353 to 403 K, an increase in the current at positive biases and minimal change in the current at negative biases were observed. Figure 4b illustrates the corresponding RR values at varying temperatures, indicating an increase in RR with increasing temperature. This single-molecule rectifier yielded an RR value of ∼750 under a bias of 1.0 V at 403 K. The RR was further increased to a maximum of ∼3519 and an average of ∼3248 at a bias of 2.0 V at 353 K (Figure S22).

https://doi.org/10.1021/jacs.5c00566
J. Am. Chem. Soc. 2025, 147, 16972−16981

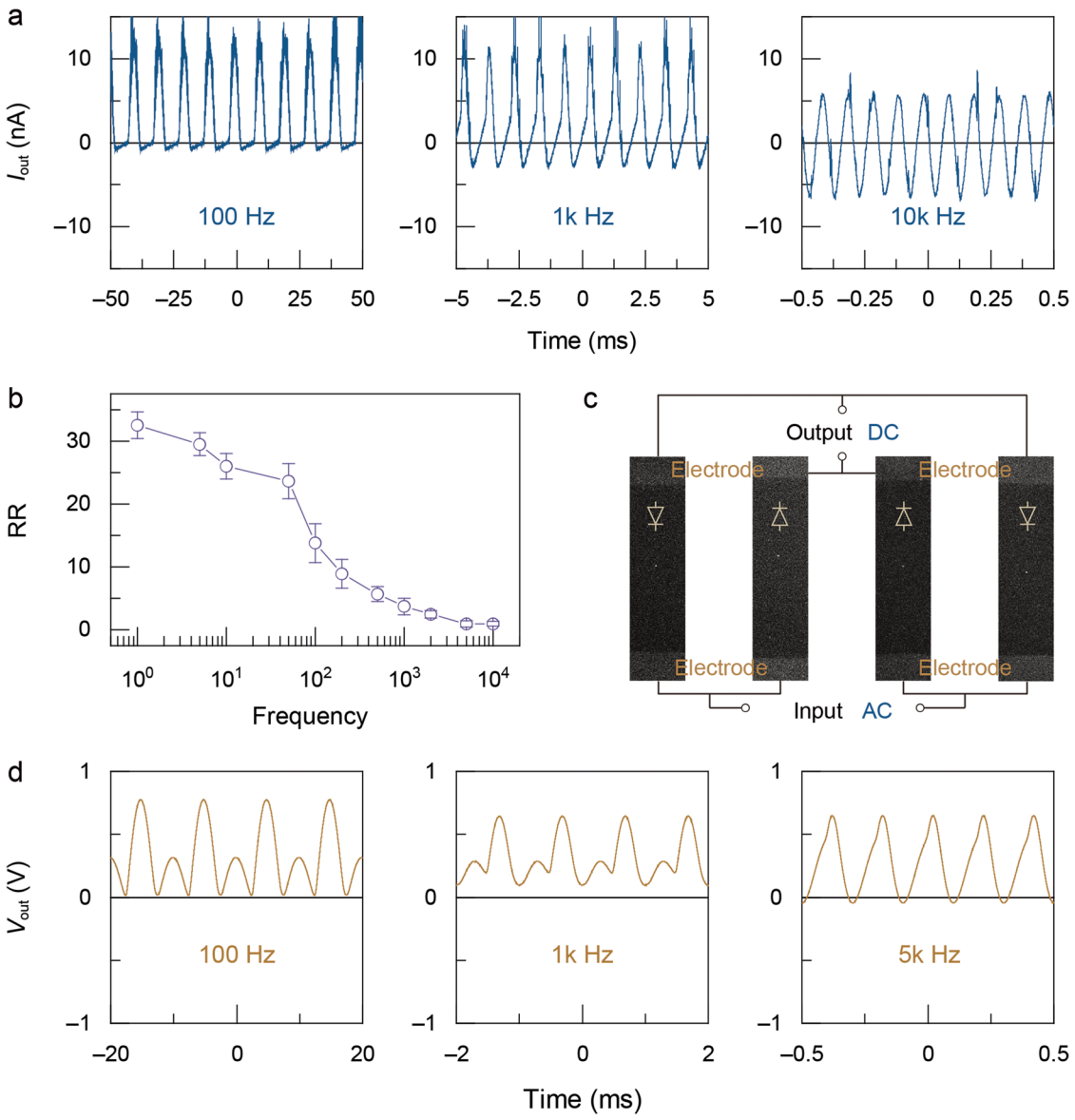

Figure 5. Alternating current-to-direct current power conversion. (a) Plots of output current (I_{out}) versus time for different frequencies of input voltage (V_{in}). V_{in} was a sinusoidal waveform with a peak voltage of 0.5 V. (b) The corresponding RR vs the frequency of V_{in}. (c) Schematic of the construction of a bridge rectifier, consisting of four rectifiers arranged in a closed loop. Superhigh-resolution images of four rectifiers are provided. Laser: 405 nm, 5 mW. Five thousand photos were taken through a ×100 oil lens with an exposure time of 50 ms. (d) Plots of output voltage (V_{out}) versus time for different frequencies of V_{in}. V_{in} was a sinusoidal waveform with a peak voltage of 1.0 V.

Furthermore, as previously mentioned, the turning point (RR = 1) of the current change lies in the low bias region due to the transition zone of structural switching between RS and PS. Statistical analyses (involving the device shown in Figure 4a,b and two additional devices shown in Figures S23 and S24) reveal a clear correlation between the turning point and temperature, with the bias at the turning point decreasing with increasing temperature (Figure 4c). The shift in turning point suggests that the temperature increase accelerates the transition between RS and PS, which is consistent with the chemical kinetics.

A comprehensive analysis of $I-V$ characteristics was undertaken to gain a fundamental understanding of the charge transport mechanism. We extracted I_{SD} at +1.0 and −1.0 V and plotted ln (I_{SD}) versus $1/T$, as shown in Figure 4d. The statistical results indicate that the current at the negative bias is independent of temperature (blue), while the current at the positive bias exhibits temperature dependence (red) and can be fitted with the Arrhenius equation as follows

$$I = I_0 e^{-E_a/k_B T} \quad (2)$$

where k_B is the Boltzmann constant and I_0 is the pre-exponential factor. The activation energy (E_a) was determined to be ∼166 meV based on the fitting (gray curve). Therefore, it can be concluded that the transport transition shifts from temperature-independent coherent tunneling at the negative bias to thermally activated incoherent transport at the positive bias. Relative to the reduction of DQI by increasing the temperature,[40] the large E_a causes a stronger temperature dependence at the positive axis and results in the observed significant sensitivity of RR to temperature.

Lewis-acidity-dependent measurements were also performed to investigate the effect of Lewis acid (LA) on rectification

https://doi.org/10.1021/jacs.5c00566
J. Am. Chem. Soc. 2025, 147, 16972−16981

performance. The statistically averaged $I-V$ curves at 373 K, in the absence and presence of LA, are presented in Figure 4e−h (detailed $I-V$ curves and corresponding RR values for multiple devices are provided in Figures S25−S44). The experimental results indicate that the presence of LA significantly increases the rectification ratio of the single-molecule rectifier in comparison with that (∼437) observed without LA (Figure 4i). Moreover, the RR increases as the LA strength increases along the series $SnCl_4$ < $TiCl_4$ < $AlCl_3$ (Figure 4i). This phenomenon can be attributed to the coordination of the metal cation in LA with the hydroxyl oxygen in the PS. In general, the conjugation effect of side groups (hydroxyl group) on the PS weakens the DQI effect,[41] thereby hindering the reduction of off-state current. The coordination mitigates this weakening effect, thus enhancing the DQI of the PS and consequently improving the rectification performance. Under the coordination effect of $AlCl_3$, the RR reaches an average value of ∼5080 and a maximum value of ∼6400 at a V_{SD} of ±1 V. In comparison with other single-molecule rectifiers[13−27,42] (Figure 4j) involving the rectification mechanisms of either asymmetric molecular cores or contacts, the RR value in this work exhibits superior rectifier performance.

AC-to-DC Power Conversion. In addition to applying the DC power, the device stability allows us to convert AC to DC. The experimental results, as shown in Figure 5a, illustrate the output current (I_{out}) as a function of time for different frequencies of input voltage (V_{in}) (detailed results are provided in Figures S45 and S46). V_{in} was a sinusoidal waveform with a peak voltage of 0.5 V. The AC-to-DC power conversion measurements showed half-wave rectification, where only the positive half-cycle of the sinusoidal input wave is converted into the output signal. At a V_{in} with a frequency of 100 Hz, the negative voltage component of the input signal was nearly completely rectified, and only the positive component could be transmitted through the single-molecule device (Figure 5a, top panel), resulting in an RR of ∼13.8 (Figure 5b). As the frequency of the AC input increased to 1000 Hz, the peak value of I_{out} at the positive bias was ∼11.5 nA, while it was ∼2.9 nA at the negative bias caused by delayed rearrangement and inherent capacitance (Figure 5a, middle panel), yielding an RR of ∼4.0. As shown in Figure 5b, the AC-to-DC conversion characteristics of this device show a trend of decreasing RR values with an increase in the frequency of the AC input, demonstrating a frequency of ∼50 Hz at −3 dB RR and a cutoff frequency at 10k Hz (RR = 1). In specific, at a V_{in} with a frequency of 10k Hz, the peak value of I_{out} at both positive and negative biases was nearly identical (Figure 5a, bottom panel), suggesting a significant reduction in the rectification capability of the device. Consequently, the range of the operational frequency of the proposed single-molecule rectifier was determined to be between 1 Hz and 10 kHz. Considering that only one molecule is involved in this AC-to-DC converter, its ability to function at high operational frequencies offers a promising avenue for future integration into electronic devices, highlighting its potential for enhancing the efficiency and miniaturization of electronic components.

Moreover, we integrated four single-molecule rectifiers into a bridge rectifier on one chip, significantly enhancing both the efficiency and the stability of the output by processing both halves of an AC waveform. Figure 5c illustrates the fundamental structure of the bridge rectifier consisting of four rectifiers arranged in a closed loop. These rectifiers were strategically oriented to allow the current to flow in a specific direction. The arrangement comprises two rectifiers connected to each AC input and two diodes directing the output, thereby ensuring that no matter the polarity of the input AC voltage, the output remains in a single and steady direction. The experimental results illustrate the output voltage (V_{out}) as a function of time for different frequencies of V_{in} as shown in Figure 5d (detailed results are provided in Figures S47 and S48). The applied V_{in} was a sinusoidal waveform with a peak voltage of 1.0 V. Specifically, at a V_{in} with a frequency of 100 Hz, the output frequency of 200 Hz was twice that of the input, exhibiting the capability of integrated molecular rectifiers to handle full-wave rectification (Figure 5d, left panel). Note that variations in the peak values of the output voltage may originate from the individual differences among the four single-molecule devices. As the frequency of V_{in} increased to 1000 Hz, there was a decrease in averaged V_{out} in comparison with the results at the 100 Hz V_{in} (Figure 5d, middle panel), indicating the performance degradation. Furthermore, at a V_{in} with a frequency of 5k Hz, the output frequency was equal to the input frequency, suggesting a loss of the full-wave rectification capability (Figure 5d, right panel). Despite the relatively low output voltage, the integration of single-molecule rectifiers into a bridge rectifier marks a pioneering advancement, potentially paving the way for future integrated electronic applications.

CONCLUSIONS

We have demonstrated a reliable single-molecule rectifier featuring a superhigh rectification ratio and effective AC-to-DC conversion capabilities. The key to our success is to utilize electric-field-catalyzed Fries rearrangement to facilitate the switching between the substrate with CQI and the product with DQI, thus providing a stable and reproducible rectification performance. Furthermore, the single-molecule rectifier exhibits a half-wave rectification behavior within an operational frequency range from 1 Hz to 10 kHz, marking a substantial achievement considering the single-molecule nature of the system. Our research is further progressed by integrating four single-molecule rectifiers into a bridge rectifier configuration, proving the integrability. This setup not only improves the overall efficiency and output stability but also utilizes both halves of the AC waveform, demonstrating the prowess of full-wave rectification.

We also note that the influence on the QIE by the side group, i.e., the conjugative effect of the hydroxyl group on the DQI PS, would weaken the rectification, which can be eliminated by LA coordination of the hydroxyl group to some extent. Therefore, the development of organic methodologies will further guide the design of single-molecule electronic components and then realize CQI and DQI switching with a higher on−off ratio to be used in either rectifiers or field effect transistors.

This advancement underscores the big potential of these devices driven by chemical reactions in boosting the efficiency and facilitating miniaturization of electronic components. Furthermore, the RR can be tuned by separately regulating the electron transport properties of the corresponding structures via external stimuli. We anticipate that the integration of diverse strategies, including the switching in charge transport mechanisms,[43] will further enhance the performance of molecular devices, making them strong candidates for programmable electronic devices. Additionally, our findings also highlight the essential balance between functionality and operational frequency, which is pivotal in shaping design and

https://doi.org/10.1021/jacs.5c00566
J. Am. Chem. Soc. 2025, 147, 16972−16981

application strategies for future molecular-based electronic devices.

■ ASSOCIATED CONTENT

Supporting Information

The Supporting Information is available free of charge at https://pubs.acs.org/doi/10.1021/jacs.5c00566.

Schematic of a single-molecule junction; experimental methods; *I*−*V* curves of single-molecule devices; single-molecule connection analysis; computational analysis of the quantum interference effect; *I*−*V* curves with different rectification directions; computational potential energy profiles; bias-voltage-dependent measurements; control experiments; IETS characterization of the conductance states; dwell times of two states in bias-voltage-dependent measurements; the rectification performance at 2.0 V; temperature-dependent measurements; Lewis-acid-assisted rectification performance; frequency-dependent measurements in the AC-to-DC conversion; and Cartesian coordinates and energies of optimized structures (PDF)

■ AUTHOR INFORMATION

Corresponding Authors

Kendall N. Houk − *Department of Chemistry and Biochemistry, University of California, Los Angeles, California 90095-1569, United States;* orcid.org/0000-0002-8387-5261; Email: houk@chem.ucla.edu

Xuefeng Guo − *Beijing National Laboratory for Molecular Sciences, National Biomedical Imaging Center, College of Chemistry and Molecular Engineering, Peking University, Beijing 100871, P. R. China; Center of Single-Molecule Sciences, Frontiers Science Center for New Organic Matter, College of Electronic Information and Optical Engineering, Nankai University, Tianjin 300350, P. R. China;* orcid.org/0000-0001-5723-8528; Email: guoxf@pku.edu.cn

Authors

Yilin Guo − *Beijing National Laboratory for Molecular Sciences, National Biomedical Imaging Center, College of Chemistry and Molecular Engineering, Peking University, Beijing 100871, P. R. China*

Chen Yang − *Beijing National Laboratory for Molecular Sciences, National Biomedical Imaging Center, College of Chemistry and Molecular Engineering, Peking University, Beijing 100871, P. R. China*

Shuyao Zhou − *Beijing National Laboratory for Molecular Sciences, National Biomedical Imaging Center, College of Chemistry and Molecular Engineering, Peking University, Beijing 100871, P. R. China; State Key Laboratory of Physical Chemistry of Solid Surfaces, College of Chemistry and Chemical Engineering, Xiamen University, Xiamen 361005, P. R. China; Department of Chemistry and Biochemistry, University of California, Los Angeles, California 90095-1569, United States*

Complete contact information is available at: https://pubs.acs.org/10.1021/jacs.5c00566

Author Contributions

⊥Y.G., C.Y., and S.Z. contributed equally to this work.

Notes

The authors declare no competing financial interest.

■ ACKNOWLEDGMENTS

The authors acknowledge primary financial support from the National Key R&D Program of China (2022YFE0128700, 2023YFF1205803, and 2021YFA1200101), the National Natural Science Foundation of China (22150013 and 21933001), the Beijing National Laboratory for Molecular Sciences (BNLMS-CXXM-202407), the NSF (CHE-2153972), and computational resources from Expanse at SDSC through allocation CHE040014 from the Advanced Cyberinfrastructure Coordination Ecosystem: Services & Support (ACCESS) program. C.Y. appreciates the support from the China National Postdoctoral Program for Innovative Talents (BX20220014), the National Natural Science Foundation of China (22303003), and the General Project of China Postdoctoral Science Foundation (2023M730049). Y.G. appreciates the support from the China National Postdoctoral Program for Innovative Talents (BX20230024) and the General Project of China Postdoctoral Science Foundation (2023M740065). S.Z. appreciates the support from the High-performance Computing Platform of the Center for Life Science (Peking University) and the High-performance Computing Platform of Peking University.

■ REFERENCES

(1) Nature editorial. There's more to come from Moore. *Nature* **2015**, *520*, No. 408.

(2) Lörtscher, E. Wiring molecules into circuits. *Nat. Nanotechnol.* **2013**, *8*, 381−384.

(3) Xiang, D.; Wang, X.; Jia, C.; Lee, T.; Guo, X. Molecular-scale electronics: From concept to function. *Chem. Rev.* **2016**, *116*, 4318−4440.

(4) Yuan, M.; Qiu, Y.; Gao, H.; Feng, J.; Jiang, L.; Wu, Y. Molecular electronics: From nanostructure assembly to device integration. *J. Am. Chem. Soc.* **2024**, *146*, 7885−7904.

(5) Xin, N.; Guan, J.; Zhou, C.; Chen, X.; Gu, C.; Li, Y.; Ratner, M. A.; Nitzan, A.; Stoddart, J. F.; Guo, X. Concepts in the design and engineering of single-molecule electronic devices. *Nat. Rev. Phys.* **2019**, *1*, 211−230.

(6) Flood, A. H.; Stoddart, J. F.; Steuerman, D. W.; Heath, J. R. Whence molecular electronics? *Science* **2004**, *306*, 2055−2056.

(7) Aviram, A.; Ratner, M. A. Molecular rectifiers. *Chem. Phys. Lett.* **1974**, *29*, 277−283.

(8) Gupta, R.; Fereiro, J. A.; Bayat, A.; Pritam, A.; Zharnikov, M.; Mondal, P. C. Nanoscale molecular rectifiers. *Nat. Rev. Chem.* **2023**, *7*, 106−122.

(9) Cao, W.; Bu, H.; Vinet, M.; Cao, M.; Takagi, S.; Hwang, S.; Ghani, T.; Banerjee, K. The future transistors. *Nature* **2023**, *620*, 501−515.

(10) Perrin, M. L.; Burzurí, E.; van der Zant, H. S. J. Single-molecule transistors. *Chem. Soc. Rev.* **2015**, *44*, 902−919.

(11) Metzger, R. M. Unimolecular electrical rectifiers. *Chem. Rev.* **2003**, *103*, 3803−3834.

(12) Elbing, M.; Ochs, R.; Koentopp, M.; Fischer, M.; von Hänisch, C.; Weigend, F.; Evers, F.; Weber, H. B.; Mayor, M. A single-molecule diode. *Proc. Natl. Acad. Sci. U.S.A.* **2005**, *102*, 8815−8820.

(13) Perrin, M. L.; Galán, E.; Eelkema, R.; Thijssen, J. M.; Grozema, F.; van der Zant, H. S. J. A gate-tunable single-molecule diode. *Nanoscale* **2016**, *8*, 8919−8923.

(14) Handayani, M.; Tanaka, H.; Katayose, S.; Ohto, T.; Chen, Z.; Yamada, R.; Tada, H.; Ogawa, T. Three site molecular orbital controlled single-molecule rectifiers based on perpendicularly linked porphyrin−imide dyads. *Nanoscale* **2019**, *11*, 22724−22729.

(15) Hihath, J.; Bruot, C.; Nakamura, H.; Asai, Y.; Díez-Pérez, I.; Lee, Y.; Yu, L.; Tao, N. Inelastic transport and low-bias rectification in a single-molecule diode. *ACS Nano* **2011**, *5*, 8331−8339.
(16) Lörtscher, E.; Gotsmann, B.; Lee, Y.; Yu, L.; Rettner, C.; Riel, H. Transport properties of a single-molecule diode. *ACS Nano* **2012**, *6*, 4931−4939.
(17) Díez-Pérez, I.; Hihath, J.; Lee, Y.; Yu, L.; Adamska, L.; Kozhushner, M. A.; Oleynik, I. I.; Tao, N. Rectification and stability of a single molecular diode with controlled orientation. *Nat. Chem.* **2009**, *1*, 635−641.
(18) Yee, S. K.; Sun, J.; Darancet, P.; Tilley, T. D.; Majumdar, A.; Neaton, J. B.; Segalman, R. A. Inverse rectification in donor−acceptor molecular heterojunctions. *ACS Nano* **2011**, *5*, 9256−9263.
(19) Zhang, N.; Lo, W.-Y.; Cai, Z.; Li, L.; Yu, L. Molecular rectification tuned by through-space gating effect. *Nano Lett.* **2017**, *17*, 308−312.
(20) Batra, A.; Darancet, P.; Chen, Q.; Meisner, J. S.; Widawsky, J. R.; Neaton, J. B.; Nuckolls, C.; Venkataraman, L. Tuning rectification in single-molecular diodes. *Nano Lett.* **2013**, *13*, 6233−6237.
(21) Van Dyck, C.; Ratner, M. A. Molecular Rectifiers: A new design based on asymmetric anchoring moieties. *Nano Lett.* **2015**, *15*, 1577−1584.
(22) Wang, K.; Zhou, J.; Hamill, J. M.; Xu, B. Measurement and understanding of single-molecule break junction rectification caused by asymmetric contacts. *J. Chem. Phys.* **2014**, *141*, No. 054712.
(23) Lei, S.; Feng, W.; Li, B.; Li, Q.; Zhao, A.; Wang, B.; Yang, J.; Hou, J. G. Orbital-selective single molecule rectifier on graphene-covered Ru(0001) surface. *Appl. Phys. Lett.* **2013**, *102*, No. 163506.
(24) Zhao, J.; Zeng, C.; Cheng, X.; Wang, K.; Wang, G.; Yang, J.; Hou, J. G.; Zhu, Q. Single $C_{59}N$ molecule as a molecular rectifier. *Phys. Rev. Lett.* **2005**, *95*, No. 045502.
(25) Peiris, C. R.; Vogel, Y. B.; Le Brun, A. P.; Aragonès, A. C.; Coote, M. L.; Díez-Pérez, I.; Ciampi, S.; Darwish, N. Metal−single-molecule−semiconductor junctions formed by a radical reaction bridging gold and silicon electrodes. *J. Am. Chem. Soc.* **2019**, *141*, 14788−14797.
(26) Capozzi, B.; Xia, J.; Adak, O.; Dell, E. J.; Liu, Z.-F.; Taylor, J. C.; Neaton, J. B.; Campos, L. M.; Venkataraman, L. Single-molecule diodes with high rectification ratios through environmental control. *Nat. Nanotechnol.* **2015**, *10*, 522−527.
(27) Guo, C.; Wang, K.; Zerah-Harush, E.; Hamill, J.; Wang, B.; Dubi, Y.; Xu, B. Molecular rectifier composed of DNA with high rectification ratio enabled by intercalation. *Nat. Chem.* **2016**, *8*, 484−490.
(28) Chen, X.; Roemer, M.; Yuan, L.; Du, W.; Thompson, D.; del Barco, E.; Nijhuis, C. A. Molecular diodes with rectification ratios exceeding 10^5 driven by electrostatic interactions. *Nat. Nanotechnol.* **2017**, *12*, 797−803.
(29) Nijhuis, C. A.; Reus, W. F.; Siegel, A. C.; Whitesides, G. M. A molecular half-wave rectifier. *J. Am. Chem. Soc.* **2011**, *133*, 15397−15411.
(30) Li, T.; Bandari, V. K.; Hantusch, M.; Xin, J.; Kuhrt, R.; Ravishankar, R.; Xu, L.; Zhang, J.; Knupfer, M.; Zhu, F.; Yan, D.; Schmidt, O. G. Integrated molecular diode as 10 MHz half-wave rectifier based on an organic nanostructure heterojunction. *Nat. Commun.* **2020**, *11*, No. 3592.
(31) Cao, Z.; Xie, Y.; Lin, J.-L.; Zhong, S.; Yan, C.; Yang, Z.; Li, M.; Zhou, Z.; Peng, W.; Qiu, S.; Liu, J.; Li, Y. Flexible crossbar molecular devices with patterned egain top electrodes for integrated all-molecule-circuit implementation. *Adv. Mater.* **2024**, *36*, No. 2406456.
(32) Markussen, T.; Stadler, R.; Thygesen, K. S. The Relation between structure and quantum interference in single molecule junctions. *Nano Lett.* **2010**, *10*, 4260−4265.
(33) Kiguchi, M.; Nakamura, H.; Takahashi, Y.; Takahashi, T.; Ohto, T. Effect of anchoring group position on formation and conductance of a single disubstituted benzene molecule bridging Au electrodes: Change of conductive molecular orbital and electron pathway. *J. Phys. Chem. C* **2010**, *114*, 22254−22261.
(34) Guo, Y.; Yang, C.; Li, H.; Zhang, L.; Zhou, S.; Zhu, X.; Fu, H.; Li, Z.; Liu, Z.; Jia, C.; Liu, Z.; Zhu, W.; Mo, F.; Zhang, D.; Guo, X. Accurate single-molecule kinetic isotope effects. *J. Am. Chem. Soc.* **2022**, *144*, 3146−3153.
(35) Yang, C.; Liu, Z.; Li, Y.; Zhou, S.; Lu, C.; Guo, Y.; Ramirez, M.; Zhang, Q.; Li, Y.; Liu, Z.; Houk, K. N.; Zhang, D.; Guo, X. Electric field−catalyzed single-molecule Diels-Alder reaction dynamics. *Sci. Adv.* **2021**, *7*, No. eabf0689.
(36) Chen, H.; Jia, C.; Zhu, X.; Yang, C.; Guo, X.; Stoddart, J. F. Reactions in single-molecule junctions. *Nat. Rev. Mater.* **2023**, *8*, 165−185.
(37) Yoshizawa, K. An orbital rule for electron transport in molecules. *Acc. Chem. Res.* **2012**, *45*, 1612−1621.
(38) Liu, J.; Huang, X.; Wang, F.; Hong, W. Quantum interference effects in charge transport through single-molecule junctions: Detection, manipulation, and application. *Acc. Chem. Res.* **2019**, *52*, 151−160.
(39) Zhao, X.; Geskin, V.; Stadler, R. Destructive quantum interference in electron transport: A reconciliation of the molecular orbital and the atomic orbital perspective. *J. Chem. Phys.* **2017**, *146*, No. 092308.
(40) Chen, Z.; Grace, I. M.; Woltering, S. L.; Chen, L.; Gee, A.; Baugh, J.; Briggs, G. A. D.; Bogani, L.; Mol, J. A.; Lambert, C. J.; Anderson, H. L.; Thomas, J. O. Quantum interference enhances the performance of single-molecule transistors. *Nat. Nanotechnol.* **2024**, *19*, 986−992.
(41) Jiang, F.; Trupp, D. I.; Algethami, N.; Zheng, H.; He, W.; Alqorashi, A.; Zhu, C.; Tang, C.; Li, R.; Liu, J.; Sadeghi, H.; Shi, J.; Davidson, R.; Korb, M.; Sobolev, A. N.; Naher, M.; Sangtarash, S.; Low, P. J.; Hong, W.; Lambert, C. J. Turning the tap: Conformational control of quantum interference to modulate single-molecule conductance. *Angew. Chem., Int. Ed.* **2019**, *58*, 18987−18993.
(42) Xin, N.; Hu, C.; Al Sabea, H.; Zhang, M.; Zhou, C.; Meng, L.; Jia, C.; Gong, Y.; Li, Y.; Ke, G.; He, X.; Selvanathan, P.; Norel, L.; Ratner, M. A.; Liu, Z.; Xiao, S.; Rigaut, S.; Guo, H.; Guo, X. Tunable symmetry-breaking-induced dual functions in stable and photoswitched single-molecule junctions. *J. Am. Chem. Soc.* **2021**, *143*, 20811−20817.
(43) Han, Y.; Nickle, C.; Maglione, M. S.; Karuppannan, S. K.; Casado-Montenegro, J.; Qi, D.-C.; Chen, X.; Tadich, A.; Cowie, B.; Mas-Torrent, M.; Rovira, C.; Cornil, J.; Veciana, J.; del Barco, E.; Nijhuis, C. A. Bias-polarity-dependent direct and inverted marcus charge transport affecting rectification in a redox-active molecular junction. *Adv. Sci.* **2021**, *8*, No. 2100055.

https://doi.org/10.1021/jacs.5c00566
J. Am. Chem. Soc. 2025, 147, 16972−16981